Parametric Redesign of a Convergent-Divergent Cold Spray Nozzle

Florentina-Luiza Zavalan[1] and Aldo Rona[2]
University of Leicester, Leicester, United Kingdom
[1] flz1@leicester.ac.uk, [2] aldo.rona@leicester.ac.uk

Abstract

The generation of a high velocity carrier gas flow for cold metal particle applications is addressed, with specific focus on titanium cold spraying. The high hardness of this material makes cold spraying titanium difficult to achieve by industry standard nozzles. The redesign of a commercial conical convergent-divergent cold spray nozzle is achieved by application of aerospace design codes, based on the Method of Characteristics, towards producing a more isentropic expansion by contouring the nozzle walls. Steady three-dimensional RANS SST k-ω simulations of nitrogen are coupled two-way to particle parcel tracking in the Lagrangian frame of reference. The new contoured nozzle is found to produce higher particle velocities with greater radial spread, when operated at the same conditions/cost of operation as the commercial nozzle. ~~The results of numerical modelling showed~~ the potential for extending cold spray to high density and low ductility particles by relatively minor rig modifications, through an effective synergy between gas dynamics and material science.

Introduction

Cold spraying is a material deposition process developed about 40 years ago by the Russian scientists as a metal coating technology [1, 2]. This technique consists in accelerating powder particles to a high velocity (typically higher than 300 m/s) by a high-speed flow. The particles impinge onto a substrate, where they plastically deform under the action of their own kinetic energy and form a coating, as shown diagrammatically in Fig. 1.

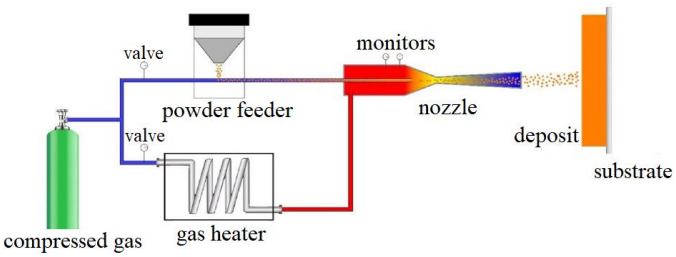

Figure 1: Schematic of a high-pressure cold spray system [3].

The major advantage of this metal processing technique is the low temperature involved, which minimizes any potential phase change of the substrate and keeps the particles in their solid state. This is making cold spray suitable for depositing a wide range of traditional and advanced materials on many types of substrate, lately being also used as an additive manufacturing and repair technology [3-5]. Alkhimov et al. [2] demonstrated that the key parameters for the successful bonding of the particles with the substrate are impact velocity and temperature. High velocity is necessary for optimal deposition efficiency and packing density. At low temperatures, particle oxidation is avoided, which can make cold spray depositions more durable and with a better bond strength. Given the key role of particle velocity and of particle kinetic energy on the quality of the deposition, a good understanding of the factors that affect the particle velocity upon impact is crucial for improving the current cold spray practices.

One of the most important components of the cold spray system is the supersonic nozzle and its capability of generating high deposition efficiency. In cold spraying, a supersonic gas jet is formed using a de Laval or a similar converging-diverging nozzle. The influence of the nozzle design in the cold spray process is discussed by several authors in the literature, with several studies dedicated to the optimization of the cold spray nozzle configuration. Dykhuizen et al. [6] presented a method for the optimal design of a cold spray nozzle. Alkimov et al. [7] also investigated a model to optimize the nozzle geometry. Later, various nozzle shapes were investigated, such as convergent-divergent nozzles [8-12], convergent-divergent-barrel nozzles [10], convergent-barrel [10, 13], and bell-shaped nozzles [14, 15]. Tabbara et al. [16] and Yin et al. [17] investigated the effect of the nozzle cross-section on the particle velocity and distribution. Suo et al. [18] and Varadaraajan et al. [19] studied the effect of the nozzle geometry on particle distribution for rectangular nozzles. Jodoin [20] found that an exit Mach number between 1.5 and 3.0 can ensure the sprayed particles achieve a sufficient deceleration on impact to provide a well-bedded metal coating. Grujicic et al. [21] discovered that a relative Mach number of 1.4 leads to the highest particle acceleration, which is conducive to generating high particle kinetic energy. These particles embed well into the target. Lupoi [22] has shown that the effect of nozzle geometry on deposition efficiency is difficult to predict.

There are still some unanswered questions concerning the influence of the nozzle design on the discrete phase properties, that is, on the particulate. Therefore, further studies are necessary to determine the optimal design approach for cold spray nozzles. ~~The current work discusses an alternative~~ workflow to designing contoured axisymmetric nozzles (the

so-called bell-shaped nozzles) for cold spraying. By Computational Fluid Dynamics (CFD), the performance of a commercial conical convergent-divergent cold spray nozzle is compared ~~with~~ that of a new nozzle profile designed with a smooth throat and for a parallel (axial) outflow. The new nozzle geometry was designed in order to improve the deposition efficiency, reduce the particle-to-particle variation in impact velocity, and produce a more even coating. The CONTUR code by Sivells [23] is used to calculate the divergent section profile of the new convergent-divergent nozzle. This code is linked to the code developed by Alcenius and Schneider [24] for calculating the nozzle convergent section profile.

In this study, a three-dimensional CFD model is developed to assess the flow and particle behaviour in a lightly laden jet, in which well-dispersed titanium particles are accelerated by a compressible flow. ANSYS FLUENT® v19.5 is used as the CFD solver. The Reynolds-Averaged Navier–Stokes (RANS) SST k-ω model is used to account for the effect of turbulence on the time-averaged state of the continuous phase and the Discrete Phase Model (DPM) is used to compute the motion of the particles.

This paper investigates specifically the effect of the nozzle geometry on the particle velocity distribution and on their radial spread. The comparison of the performance of the two nozzles is performed at the same operating conditions and for the same particle size distribution. The intent is to compare the impingement patterns of the metal deposition at the same cost of nitrogen gas supply and of the particle powder supply.

Nozzle design

In order to maximize the spray particle acceleration from the particle feeder to the substrate target, an axisymmetric nozzle with contoured walls is proposed, to replace the conical convergent-divergent shape of the Out4 nozzle (Fig. 2) in current use by industry. This is achieved by adapting compressible flow design methods originally developed for transonic and supersonic wind tunnel nozzles. This technique aims at improving the radial uniformity of the outflow velocity, compared to the more established conical cold spray nozzle design. The idea is to optimize the conventional nozzle geometry to produce higher quality flow under the same nozzle inflow conditions.

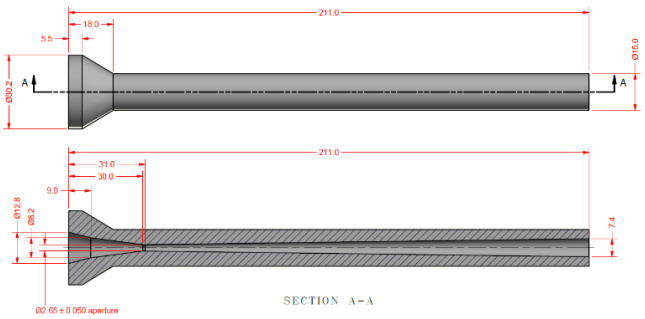

Figure 2: Out4 convergent-divergent cold spray nozzle [25].

The design of the new nozzle is obtained by using the CONTUR code [23] in conjunction with the code developed by Alcenius and Schneider [24]. CONTUR uses a combination of analytical solutions, the Method of Characteristics (MOC), and prescribed centreline distributions of axial velocity ~~in order~~ to determine the divergent section profile of a convergent-divergent de Laval nozzle. This is a FORTRAN 77 code which runs through a series of 16 subroutines and uses seven user-defined input cards, which describe the desired flow conditions through the nozzle. These cards are provided as a seven-line formatted ASCII text input file that is read at run time. A detailed description of the code is given in [23]. The code is capable of designing either axisymmetric or planar nozzles with a supersonic outflow and has been successfully used in previous work [26, 27]. The convergent part of the nozzle is obtained by the complementary code of Alcenius and Schneider [24] which uses the Hopkins and Hill [28] perturbation solution for the flow in the transonic region of an axisymmetric nozzle. By combining the two codes, the entire axisymmetric nozzle wall profile is determined.

The authors translated and updated the original codes from FORTRAN 77 to FORTRAN 90, creating a shareable software library able to run on high-performance computer clusters. The CONTUR code library is available both through GitHub under the keyword CONTUR and it is also distributed as Research Data associated to this publication. The FORTRAN 90 code was shown to reproduce exactly the reference numerical (tabulated) solution of the original FORTRAN 77 code for a Mach 4.0 nozzle [23]. The coupling between the geometrical profiles of the convergent and of the divergent sections required additional work, due to the code of Alcenius and Schneider giving an inviscid flow prediction, whereas CONTUR allows for the boundary layer displacement thickness growth along the nozzle walls. A curvature-based design approach is adopted, by which the curvature value from the CONTUR code is matched analytically and exactly at the throat, by scaling the curvature of the Alcenius and Schneider [24] code profile output.

Numerical model

Computational domain and boundary conditions

The geometry of a cold spray nozzle representative of current cold spray technology provides the baseline for designing a nozzle with enhanced performance. The selected baseline geometry is a convergent-divergent nozzle, specifically, the Out4 nozzle manufactured for the Impact Innovations 5/11 cold spray system from Impact Innovations GmbH. The nozzle geometry details, obtained by measuring up a used Out4 nozzle to ±0.1 mm at The Welding Institute, are presented in Fig. 2. The nozzle discharge is modelled in the computational domain of Fig. 3. A full three-dimensional computation is performed in the computational domain that is axisymmetric about the nozzle axis. For simplicity, Fig. 3 shows only ~~the~~ half of the computational domain through the nozzle meridional plane. The computational domain extends axially by 400 mm from the nozzle exit plane and the radial extent of

the computational domain is 300 mm. Figure 3 uses broken lines along inlet 2, the far-field, and the outlet boundaries to indicate that the far-field and outlet boundaries are located farther. The far-field boundary is located about 2.3 times farther and the outlet boundary is located about 4 times farther than what is shown in this sketch.

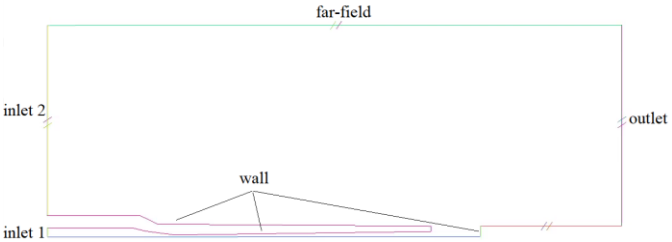

Figure 3: Sketch of the computational domain and boundaries.

A gas settling chamber of 60 mm axial length feeds the nozzle inlet, which is the start of the convergent nozzle section shown in Fig. 3, to the right of the computational domain inlet 1. The axial particle feeder has a diameter of 4 mm and it is located at the nozzle inlet. The substrate, that is the cold spray coating target, is placed at an axial distance of 35 mm to the right of the nozzle exit plane. The nozzle is supplied with compressed nitrogen and it discharges in nitrogen. Along the inlet boundaries, constant total pressure p_0 and ~~the~~ total temperature T_0 values are imposed. The values of p_0 and T_0 used along inlet 1 and inlet 2 are listed in Table 1. Along the computational domain outlet, a constant pressure outflow condition is imposed, with zero gauge pressure. The far-field boundary was placed sufficiently far from the nozzle ~~not to~~ influence significantly its streamwise growth. Along the nozzle walls and substrate, a no-slip adiabatic wall boundary condition is applied together with the trap condition to trap all the particles hitting these surfaces.

Table 1: Cold spray inlet conditions for the gas.

Boundary	**Pressure**	**Temperature**
inlet 1	5×10^6 Pa	1373.15 K
inlet 2	150 Pa	300 K

The computational domain is discretized in finite volumes using a structured multi-block body-fitted Cartesian mesh of about 1.6 million cells. This mesh is obtained by the commercial CFD mesh generator ICEM CFD® v19.5. Figure 4 shows the surface mesh of the nozzle and of the substrate with the salient details of the mesh across the nozzle throat. Radial mesh clustering is used to resolve the nozzle wall boundary layer. Axial mesh clustering is applied at the throat, at nozzle exit, and close to the substrate, in order to capture the jet shear layer and the flow characteristics of the impinging jet.

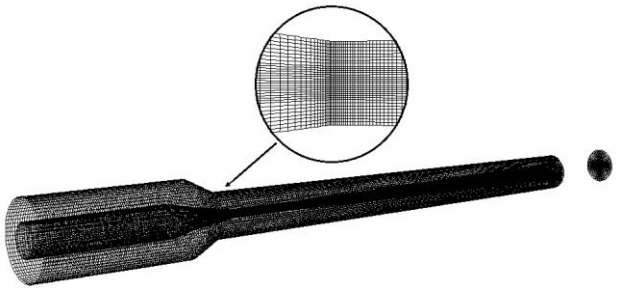

Figure 4: Computational mesh

In the computational domain, the motion of the gas flow is evaluated in the Eulerian frame of reference. Nitrogen is modelled as compressible ideal gas, at a constant specific heat ratio C_p/C_v = 1.4. The specific heat capacity is varied with temperature to account for the significant adiabatic cooling that the gas undergoes upon expansion through the nozzle. A piecewise-polynomial function with two ranges determines the specific heat capacity of nitrogen: the Andrews and Biblarz polynomial profile [29] is used over the temperature range 250 K ≤ T < 1150 K, and the NASA polynomial [30] is used over the temperature range 1150 K ≤ T < 2500 K. The viscosity is modelled by Sutherland's law. A secondary phase is introduced in the form of dispersed particles, the motion of which is solved in a Lagrangian frame of reference. Titanium particles are injected at a constant rate of 3 g/s. The material properties of the particles used in the simulation are shown in Table 2.

Table 2: Properties of the simulated powder material.

Property	**Description**
Material	Titanium (Ti)
Particle density, kg/m^3	4850
Specific heat capacity, J/kg/K	544.25
Initial particle velocity, m/s	10
Initial particle temperature, K	298.15
Critical velocity, m/s	650 [31]

Numerical scheme

The conservative laws of mass, momentum, and energy are solved for the carrier phase using the density-based implicit flow solver in ANSYS FLUENT® v19.5. The steady-state flow solution method is used. The Roe flux-difference scheme [32] is used with a third-order MUSCL interpolation by van Leer [33] to determine the fluxes of the conservative laws at the finite-volume cell faces. Turbulence is accounted for by the Shear Stress Transport (SST) k-ω model. The motion of the titanium particles is computed using the Discrete Phase Model (DPM).

This model follows the Euler-Lagrange approach: the fluid phase is treated as a continuum by solving the time-averaged Navier-Stokes equations (Eulerian reference frame), and the dispersed phase is solved by tracking a number of particles through the calculated flow field of the continuous phase (Lagrangian reference frame).

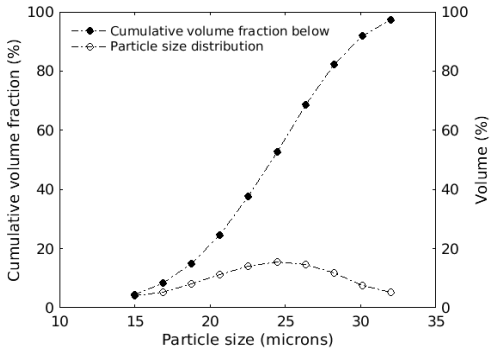

Figure 5: Distribution of particle size for the titanium powder used for the cold spray simulation.

The particles used in the discrete phase model are assumed spherical, which implies an ideal milling process. A real milling process produces particles of variable sphericity that is known to affect the particle spread [34]. Still, the spherical particles used in this model are appropriate for showing differences in the particle spray pattern from different nozzle shapes. The particle size distribution is approximated by a Rosin-Rammler distribution with the spread parameter of 5.79, as shown in Fig. 5. A sample of 5000 spherical particles is injected in the RANS converged flow solution from the nozzle inlet plane. The particle size in the sample ranges from 15 µm to 32 µm.

The particles are advanced by using the unsteady tracking method in ANSYS FLUENT. The method consists in calculating the trajectory of each particle by integrating the force balance on the particle. The high-Mach-number drag law is used for computing the drag coefficient of the particles.

This study uses a two-way coupling between the solid phase and the fluid phase, to account for the kinetic energy transfer via drag and turbulence as well as for the heat exchange between the gas and the particles. This is implemented by means of source terms of mass, momentum and energy to the conservative laws. The dispersion of the particles due to turbulent fluctuations in the flow is modelled using stochastic tracking, by the Discrete Random Walk model. This allows to predict the trajectories of particles using a reconstructed/estimated value of the instantaneous carrier phase (gas) velocity. A detailed description of these models can be found in the FLUENT User's Guide [35].

In order to quantify the improvements from the nozzle redesign, a penalty function, Φ, is evaluated for each nozzle shape. This penalty function is defined as $\Phi = a(1-Z_1) + aZ_2 + 2aZ_3$, where $a = 0.25$ is an adjustable coefficient that reflects the design intent. The first parameter, Z_1, represents the ratio of the mass-weighted particle speed evaluated just off the substrate to the maximum gas velocity. The second one, Z_2, is the mass-weighted standard deviation of the particle speed normalized by the mass-weighted mean particle speed, and the third parameter, Z_3, represents the coefficient of variation (COV), which is a point-to-point measure of the uniformity in the spread of the particles over the substrate face [36].

The simulations presented here ~~are~~ conducted on the University of Leicester high-performance computing cluster ALICE, which has 4,760 2.4GHz cores. They were performed using shared-memory parallelism using 16 cores per simulation.

Results and discussions

In this section, the results from the computational fluid dynamic simulations are organized as follows: first, the model validation for the carrier phase is presented and discussed; next, the profiles of the baseline nozzle and of the redesigned nozzle are presented and their effects on the gas velocity, particle velocity distribution, and on the particle radial spread are analysed; finally, the penalty function Φ is evaluated for the two nozzles.

In order to validate the continuous phase solver, simulations are obtained of the compressible flow generated by an infinite lipped convergent nozzle operating at a Nozzle Pressure Ratio (NPR) of 3.4. The nozzle is infinite lipped in that the nozzle discharges through a circular opening cut into a solid wall of large frontal area. The jet issuing from the nozzle impacts on a plate located at an axial distance of ~~0.5~~ nozzle exit diameters (D) from the nozzle exit plane. The numerical results are compared against the experimental data reported in Weightman et al. [37].

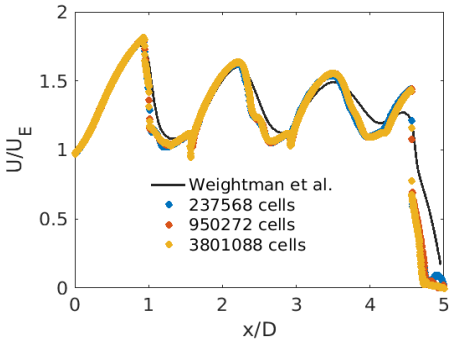

Figure 6: Axial distribution of centreline velocity from PIV [37] (line) and CFD (symbols) for three levels of computational mesh refinement.

Figure 6 shows by a continuous line the centreline velocity obtained from the Particle Image Velocimetry (PIV) velocity vector fields [37] and by symbols the centreline velocity obtained from three different computational mesh refinement levels. The velocities are nondimensionalized by the choked jet exit velocity, U_E, of 310 m/s. The alternating U_E maxima and minima denote four shock cells. This shock cell sequence starts by an expansion at the nozzle exit plane that generates a maximum mean gas velocity of $1.8U_E$. This maximum is well captured in the numerical results. There are some inconsistencies between the experimental measurement and the numerical results. One possible reason could be the fact that the experimental velocity field was obtained by averaging instantaneous velocity fields and perhaps the number of samples were not sufficient to obtain a true mean velocity

field. However, the U_E trend in the CFD predictions follows satisfactorily that in the experiment as far as the shock cell train is concerned. There is good overlap among the predictions obtained with different levels of computational mesh refinement. This indicates that this predominantly inviscid flow is relatively insensitive to the mesh refinement level, which suggests that the spatial resolution on the meridional plane is appropriate for modelling this flow.

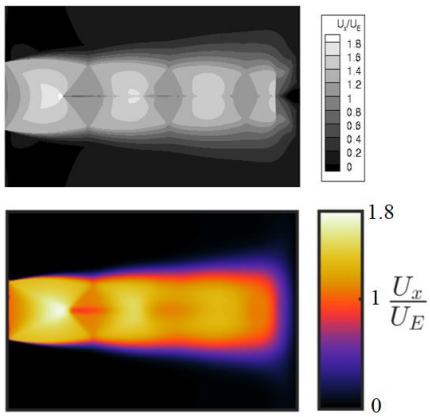

Figure 7: Greyscale levels of mean axial velocity predicted by CFD (top) and iso-colour levels of mean axial velocity from Weightman et al. [37] (bottom).

Figure 6 shows a coarser agreement between the predicted and measured axial velocity distribution at $x/D > 4$, in the impingement region approaching the target plate. The iso-levels of mean axial velocity in Fig. 7 give some insight into this discrepancy. The axisymmetric numerical prediction displays by the greyscale levels a bow shock developing just upstream of the target plate, identified by a crisp jump in the greyscale level from approximately 1.4 (light grey) to approximately 0.8 (dark grey) across this shock that stems nearly vertically from the jet axis. The corresponding experimental result shows a more gradual velocity reduction, as denoted by the axial velocity iso-colour levels changing from yellow through red and then blue. It is possible that either the lag in the PIV particle response or the azimuthal precession of the impingement region in the experiment may have smeared this compressible flow feature.

A further spatially small difference between computation and experiment is shown at the apex of the shock cones in the shock train. At this operating pressure ratio, the shock cone apex is blunt and the shock cone is closed by a small Mach disk. The iso-colour levels from experiment show the effect of the Mach disk in the first shock cell, specifically the appearance of a shear layer (shown in red) close to the nozzle axis, running parallel to the jet axis. The shear layer develops from the triple point of the lambda shock that joins the circumference of the Mach disk with the oblique shocks above it. This feature is sharper and less radially spread in the equivalent numerical predictions of Fig. 7. In Fig. 6, the 3.8M cells simulation captures the effect of this Mach disk as a localized sharp drop in axial velocity at approximately 1.8 x/D and a similar drop at 3.0 x/D suggests the presence of a second, smaller Mach disk at the apex of the shock cone of the second shock cell. The intensity and the spatial location of these compressible flow features is typically very sensitive to the nozzle pressure ratio, which always has a setting tolerance in experiment. It is therefore not surprising that these features appear more diffused in the experimental record, which uses a time average of PIV vector maps from double-exposure images to reconstruct the mean axial velocity. Specifically, any drift in the nozzle pressure ratio setting over time during the image acquisition would likely produce such effect. This may be the reason for the differences between numerical and experimental results after the first shock cell, close to the jet axis. Recalling that the Mach disk has a small radial extent, it may be argued that the selected numerical method has shown good overall predictive ability for a compressible impinging jet. On this basis, this model is taken onwards, with some confidence, for the redesign of the nozzle.

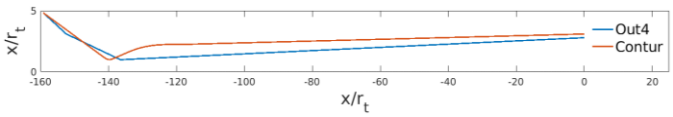

Figure 8: Nozzle profiles.

Figure 8 shows the radial profiles of the internal wall of the baseline nozzle Out4, by the blue line, and of the nozzle re-profiled using CONTUR, by the red line. It can be observed that the new nozzle was redesigned be keeping the same throat diameter and overall length as those of the industrial nozzle. The aim is to produce fully expanded outflow conditions, thereby improving the radial uniformity of the gas velocity and, consequently, of the particle velocity. The new nozzle has a convergent part 4.2 mm shorter than the baseline nozzle and an exit diameter of 8.2 mm. The baseline convergent-divergent geometry is hereafter referred to as the Out4 nozzle and the redesign output as the CONTUR nozzle.

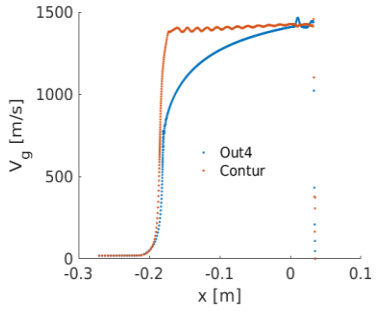

Figure 9: Velocity magnitude of the carrier gas phase along the axis of the nozzle.

Figure 9 shows that the nozzle redesign significantly changed the velocity magnitude of the carrier gas phase. An earlier Mach number rise through the nozzle is obtained by locating the throat upstream, thereby exposing the titanium particles to high drift velocities sooner through the expanding gas. This is important, since the goal is to reduce the lag between the particle speed and the gas speed at the nozzle exit, so that the

particles can be accelerated above their critical velocity, which enables them to deposit on the substrate. Figure 9 shows that the nozzle redesign produced a carrier gas acceleration to higher speeds, as shown by the red line being above the blue line inside the nozzle ($x < 0$). The redesign has also essentially removed the shocks downstream of the Out4 nozzle exit plane, up to the bow shock just in front of the substrate, as indicated by the suppression of the oscillations that are shown by the blue line at $x > 0$ that are absent from the red line at $x > 0$.

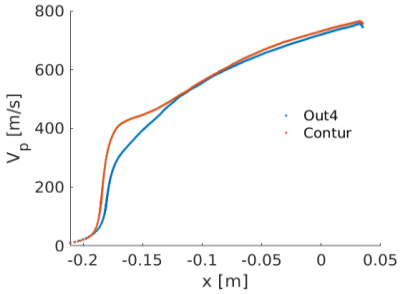

Figure 10: Velocity magnitude of a titanium particle with a diameter of 24.4 µm.

The speed change of a sample titanium particle with a diameter of 24.4 µm is shown in Fig. 10 through both nozzles. The titanium particle attains a higher velocity through the CONTUR nozzle than through the Out4 baseline nozzle, while both nozzles are operating with the same gas supply. This speed advantage is obtained throughout the particle size range 15 µm to 32 µm reported in Fig. 5. The maximum predicted particle velocity is 904.61 m/s with the Out4 nozzle, while it is 10 m/s higher with the CONTUR nozzle. The minimum predicted particle velocity is 684.41 m/s for the Out4 nozzle and 698.21 m/s for the CONTUR nozzle. This indicates a two-fold advantage delivered by the redesign. On one hand, since the peak particle velocity is directly related to the particle kinetic energy, there is potential for a more energetic plastic deformation upon impact, which may improve the metal deposition characteristics. Additionally, the removal of lower velocity particles may reduce waste of powder feed, since lower velocity particles either rebound or poorly attach to the substrate.

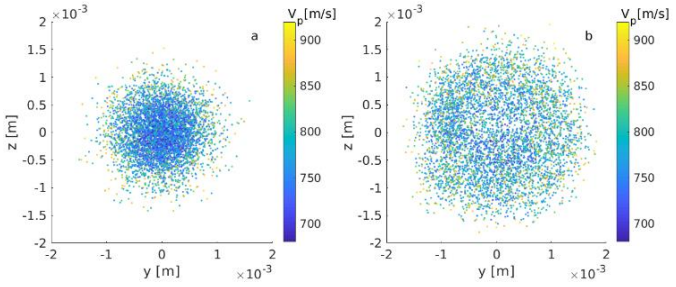

Figure 11: Radial spread of the titanium particles on impact with the substrate located at 35 mm from the nozzle exit (a) Out4 nozzle and (b) CONTUR nozzle.

By injecting the particles with the size distribution presented in Fig. 5, the particle impact patterns shown in Fig. 11 are obtained on the substrate (target) located 35 mm axially downstream of each nozzle. It can be observed that the radial distribution of the particles is also affected by the redesign, by which particles are visibly spread out more by the CONTUR nozzle. The baseline Out4 nozzle is predicted to direct most of the particles radially close to the nozzle axis, located at (y, z) = (0, 0). This is likely to cluster the particles so that some of them will strike the substrate in the same place. Over time, this particle overlap will increase the angle of the deposited material, thereby creating deposits with a conical profile, rather than an even layer, the latter being more desirable in a metal spray deposition process. Therefore, the redesigned nozzle produces a more spread out and even particle impact pattern.

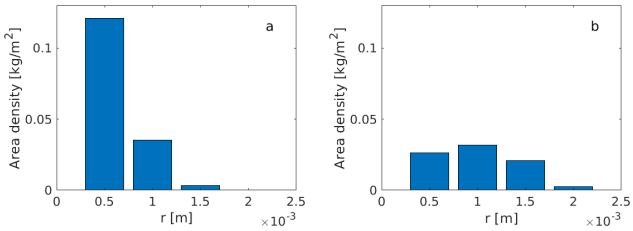

Figure 12: Area density of the titanium particles on impact with the substrate located at 35 mm from the nozzle exit (a) Out4 nozzle and (b) CONTUR nozzle.

A more quantitative measure of the uniformity of the particle distribution with the two nozzles is presented in Fig. 12. This shows the area density of titanium particles impacting the substrate shown in Fig. 11. The area density is determined by adding the mass of particles falling on concentric rings of area $2\pi r \times 0.5$ mm, divided by each ring area. It can be seen that, in the case of the Out4 nozzle, most of the mass of the injected particles accumulates on a disk of 0.5 mm radius. The area density at 1 mm mean radius reduces to less than 1/3 of that at 0.5 mm radius, indicating a rather radially uneven coating that tapers rapidly with increasing radial distance from the nozzle axis. The predicted area density of the titanium particles delivered by the CONTUR nozzle shows a more favourable radial distribution, which is more even up to 1.5 mm. Some of the benefits of using a MOC designed nozzle identified herein are consistent with the ones reported in by Gärtner et al. [14], who concludes that a MOC designed nozzle can deliver more economical process conditions and better coating qualities.

Table 3: Bulk performance of the baseline and redesigned cold spray nozzles based on the ensemble of particles impacting the substrate located 35 mm downstream of the nozzle exit plane.

	Out4	**Contur**
$Z_1 = \text{mean}(V_p)/\max(V_g)$	0.5078	0.5249
$Z_2 = \sigma(V_p)/\text{mean}(V_p)$	0.0483	0.0464
$Z_3 = COV$	0.7466	0.6559
$\Phi = 0.25(1\text{-}Z_1) + 0.25Z_2 + 0.5Z_3$	0.5084	0.4583

Table 3 compares the performance of the Out4 and of the CONTUR nozzles based on how these nozzles achieve a higher mass-averaged particle velocity relative to their maximum gas velocity, a lower mass-weighted particle velocity standard deviation, and a more uniform spatial distribution of particles on the substrate. On all three counts, the CONTUR nozzle outperforms the baseline nozzle. The mass-averaged particle velocity ratio Z_1 is 3.37% higher than that of the Out4 nozzle and the weighted standard deviation is 3.93% lower. The most significant difference between the two nozzles is in terms of the coefficient COV that expresses the departure from an even particle distribution over the substrate, this being 12.15% lower than that of the Out4 nozzle.

To compare the performance of different engineering design solutions, it is often useful to translate the desirable outcomes into numerical values that can be prioritized by weight averaging them. In this work, the authors have elected to define a penalty function Φ that the better design minimizes. Table 3 shows that, by redesigning the nozzle, its performance is improved by 9.85%, based on the change in Φ.

Conclusions

The mass transport by a lightly laden supersonic nitrogen jet was examined with the aim of generating favourable conditions for the cold spray of titanium particles. The spraying of this light material is challenging, due to its high critical velocity that prevents low-speed particles from successfully depositing on the target substrate.

Time-averaged RANS with SST k-ω turbulence closure was used to provide three-dimensional flow predictions through the Out4 nozzle, which is an industry standard geometry for cold spray applications, and the CONTUR nozzle, which is the Out4 nozzle redesigned by application of the Methods of Characteristics. A coupled Eulerian-Lagrangian particle tracking model was used to predict the motion of titanium particles through the accelerating nitrogen carrier.

The CFD predictions showed tangible improvements in the gas carrier phase flow quality. Specifically, a monotonic accelerating axial flow through the nozzle was obtained, which confers a mainly axial drift velocity to the metal particles. The outcome is a new nozzle design with a significantly reduced shock formation obtained at the same operating conditions and therefore at the same gas and particle powder supply costs used by the industry standard nozzle. The DPM predicted particles exiting the nozzle with greater velocity and with a more even particle radial spread. This is conducive to forming a more homogeneous metal deposition.

This redesign delivers a predicted performance gain of 9.85%, as evaluated from a reduction in the compound penalty from a lack of particle speed at impact, variance in the particle speed at impact, and lack of radial uniformity in the substrate coverage. This redesign has therefore shown the tangible benefit of translational application of classical compressible flow aerodynamics to metal processing. This forms a good starting point from which to further develop rig-specific modifications to enable particle deposition efficiencies with titanium that are economically viable.

Acknowledgments

The PhD research of Florentina-Luiza Zavalan is mainly funded and supported by EPSRC (EPSRC CDT Grant number EP/L016206/1) in Innovative Metal Processing. This research used the ALICE High Performance Computing Facility at the University of Leicester. Insightful guidance from P. McNutt and D. Harvey, from The Welding Institute (TWI), is gratefully acknowledged.

References

[1] A.P. Alkimov, *et al.*, "Method of Applying Coatings," Russian Patent No. 1618778, Sept 8, 1990 (Priority of the Invention: Jun 6, 1986).

[2] A.P. Alkimov, *et al.*, "A Method of Cold Gas-Dynamic Deposition," *Sov. Phys. Dokl.*, Vol. 35, No. 12 (1990), p 1047-1049.

[3] S. Yin, *et al.*, "Cold spray additive manufacturing and repair: Fundamentals and applications," *Additive Manufacturing*, Vol. 21 (2018), p 628-650. doi:10.1016/j.addma.2018.04.017

[4] A. Papyrin, *et al.*, *Cold Spray Technology*, Elsevier Science (2007). doi:10.1016/B978-0-08-045155-8.X5000-5

[5] V.F. Kosarev, *et al.*, "On Some Aspects of Gas Dynamics of the Cold Spray Process," *J. Therm. Spray Technol.*, Vol. 12 (2003), p 265-281. doi:10.1361/105996303770348384

[6] R.C. Dykhuizen and M.F. Smith, "Gas Dynamic Principles of Cold Spray," *J. Therm. Spray Technol.*, Vol. 7, No. 2 (1998), p 205-212. doi:10.1361/105996398770350945

[7] A.P. Alkhimov, *et al.*, "The Features of Cold Spray Nozzle Design," *J. Therm. Spray Technol.*, Vol. 10, No. 2 (2001), p 375-381. doi:10.1361/105996301770349466

[8] K. Sakaki and Y. Shimizu, "Effect of Increase in Entrance Length of Gun Nozzle on HVOF and Cold Spray Process," *J. Therm. Spray Technol.*, Vol. 10, No. 3 (2001), p 487-496.

[9] T. Stoltenhoff, *et al.*, "An Analysis of the Cold Spray Process and its Coatings," *J. Therm. Spray Technol.*, Vol. 11, No. 4 (2002), p 542-550.

[10] K. Sakaki, *et al.*, "Effect of nozzle geometry on cold spray process," *International Thermal Spray Conference*, Essen, Germany, March 2002, p 385–389.

[11] W-Y. Li and C-J. Li, "Optimal Design of a Novel Cold Spray Gun Nozzle at a Limited Space," *J. Therm. Spray Technol.*, Vol. 14, No. 3 (2005), p 391-396.

[12] P. Heinrich, *et al.*, "Laval Nozzle for Thermal and Kinetic Spraying," U.S. Patent 2005/0001075 A1, Jan 6, 2005.

[13] W-Y. Li, *et al.*, "Optimal Design of a Convergent-Barrel Cold Spray Nozzle by Numerical Method," *Applied Surface Science*, Vol. 253, No. 2 (2006), p 708-713.
[14] F. Gärtner, *et al.*, "The Cold Spray Process and Its Potential for Industrial Applications," *J. Therm. Spray Technol.*, Vol. 15, No. 2 (2006), p 223-232. doi:10.1361/105996306X108110
[15] T. Schmidt, *et al.*, "From Particle Acceleration to Impact and Bonding in Cold Spraying," *J. Therm. Spray Technol.*, Vol. 18, No. 5-6 (2009), p 794-808. doi:10.1007/s11666-009-9357-7
[16] H. Tabbara, *et al.*, "Study on Process Optimization of Cold Gas Spraying," *J. Therm. Spray Technol.*, Vol. 20, No. 3 (2011), p 608-620. doi:10.1007/s11666-010-9564-2
[17] S. Yin, *et al.*, "Computational analysis of the effect of nozzle cross-section shape on gas flow and particle acceleration in cold spraying," *Surf. Coatings Technol.*, Vol. 205 (2011), p 2970-2977. doi:10.1016/j.surfcoat.2010.11.002
[18] X.K. Suo, *et al.*, "Numerical study on the effect of nozzle dimension on particle distribution in cold spraying," *Surf. Coatings Technol.*, Vol. 220 (2013), p 107-111. doi:10.1016/j.surfcoat.2012.09.029
[19] V. Varadaraajan and P. Mohanty, "Design and optimization of rectangular cold spray nozzle: Radial injection angle, expansion ratio and traverse speed," *Surf. Coatings Technol.*, Vol. 316 (2017), p 246-254. doi: 10.1016/j.surfcoat.2017.03.005
[20] B. Jodoin, "Cold Spray Nozzle Mach Number Limitation," *J. Therm. Spray Technol.*, Vol. 11, No. 4 (2002), p 496-507.
[21] M. Grujicic, *et al.*, "Flow analysis and nozzle-shape optimization for the cold-gas dynamic-spray process," *Proc. Instn Mech. Engrs*, Vol. 217 (2003), p 1-11.
[22] R. Lupoi, "Current design and performance of cold spray nozzles: experimental and numerical observations on deposition efficiency and particle velocity," *Surf. Eng.*, Vol. 30, No. 5 (2014), p 316-322.
[23] J.C. Sivells, "A computer program for the aerodynamic design of axisymmetric and planar nozzles for supersonic and hypersonic wind tunnels," *ARO Inc.*, ADEC-TR-78-63 (1978).
[24] T. Alcenius and S.P. Schneider, "Status Report for NASA Langley Grant NAG-1-1133: Development of a Code for Wall Contour Design in the Transonic Region of Axisymmetric and Square Nozzles," NASA-CR-194857 (1994).
[25] P. McNutt, TWI Ltd. Granta Park, Great Abington, Cambridge, UK, personal communication (2020).
[26] J.J. Korte, "Inviscid Design of Hypersonic Wind Tunnel Nozzles for a Real Gas," *AIAA Paper 2000-0677* (2000).
[27] S.E. Adams, "The Design and Computational Validation of a Mach 3 Wind Tunnel Nozzle Contour," Master thesis, University of Tennessee, Knoxville (2016).
[28] D.F. Hopkins and D.E. Hill, "Effects of Small Radius of Curvature on Transonic Flow in Axisymmetric Nozzles," *AIAA Paper*, Vol. 4, No. 8 (1966).
[29] J.R. Andrews and O. Biblarz, "Temperature dependence of gas properties in polynomial form," *Naval Postgraduate School*, No. NPS67-81-001 (1981).
[30] B.J. McBride, *et al.*, "Coefficients for Calculating Thermodynamic and Transport Properties of Individual Species," NASA Report TM-4513 (1993).
[31] S.H. Zahiri, *et al.*, "Characterization of Cold Spray Titanium Supersonic Jet," *J. Therm. Spray Technol.*, Vol. 18, No. 1 (2009), p 110-117. doi:10.1007/s11666-008-9278-x
[32] P.L. Roe, "Approximate Riemann Solvers, Parameter Vectors and Difference Schemes," *J. Comput. Phys.*, Vol. 43 (1981), p 357-372.
[33] B. Van Leer, "Towards the ultimate conservative difference scheme. II. Monotonicity and conservation combined in a second-order scheme," *J. Comput. Phys.*, Vol. 14 (1974), p 361-370.
[34] O.Ç. Özdemir, *et al.*, "Particle Velocimetry, CFD, and the Role of Particle Sphericity in Cold Spray," *Coatings*, Vol. 10 (2020), p 1-26. doi:10.3390/coatings10121254
[35] Ansys Inc., *ANSYS FLUENT Theory Guide*, USA (2012).
[36] M.S. Ong, *et al.*, "Statistical measures of two dimensional point set uniformity," *Computational Statistics and Data Analysis*, Vol. 56 (2012), p 2159-2181.
[37] J. Weightman, *et al.*, "Effects of Nozzle Lip Thickness on the Global Modes of an Impinging Supersonic Jet," *7th Australian Conference on Laser Diagnostics in Fluid Mechanics and Combustion*, Melbourne, Australia, December 2015.